Self-bound Bose mixtures

Clemens Staudinger,[1] Ferran Mazzanti,[2] and Robert E. Zillich[1]
[1]*Institute for Theoretical Physics, Johannes Kepler University, Altenbergerstrasse 69, 4040 Linz, Austria*
[2]*Departament de Física i Enginyeria Nuclear, Campus Nord B4-B5, Universitat Politècnica de Catalunya, E-08034 Barcelona, Spain*

(Received 26 April 2018; published 31 August 2018)

Recent experiments confirmed that fluctuations beyond the mean-field approximation can lead to self-bound liquid droplets of ultradilute binary Bose mixtures. We proceed beyond the beyond-mean-field approximation and study liquid Bose mixtures by using the variational hypernetted-chain Euler–Lagrange method, which accounts for correlations nonperturbatively. Focusing on the case of a mixture of uniform density, as realized inside large saturated droplets, we study the conditions for stability against evaporation of one of the components (both chemical potentials need to be negative) and against liquid-gas phase separation (spinodal instability), the latter being accompanied by a vanishing speed of sound. Dilute Bose mixtures are stable only in a narrow range near an optimal ratio ρ_1/ρ_2 and near the total energy minimum. Deviations from a universal dependence on the s-wave scattering lengths are significant despite the low density.

DOI: 10.1103/PhysRevA.98.023633

Ultracold quantum gases provide a rich toolbox to study correlations in quantum many-body systems [1] and model condensed-matter physics such as magnetic systems [2], solid-state systems [3], or superfluidity [4]. A recent example is the prediction [5] and two independent observations [6,7] of a self-bound liquid mixture of two ultradilute Bose gases (^{39}K atoms in two different hyperfine states). In this liquid state, when the attraction between different species overcomes the single-species average repulsion, the mean-field approach [8] would predict a collapse. In Ref. [5], correlations were taken into account approximatively by using the beyond-mean-field (BMF) approximation [9], based on the Lee–Huang–Yang (LHY) expansion in a local density approximation. In a regime where the BMF corrections can stabilize the binary mixture by compensation of the mean-field attraction, self-bound droplets are formed which live long enough to perform measurements with the trapping potential switched off. Being self-bound and three dimensional, they are different from bright solitons, which are essentially one dimensional and have a limited number of particles [10], while droplets can only be formed with a critical minimum number of atoms. On a similar footage, self-bound droplets in the region of mean-field collapse have also been found in dipolar trapped systems of ^{164}Dy [11–13] and ^{166}Er [14] atoms. In this case quantum fluctuations compensate the attractive components of the dipolar interactions, as confirmed by theory [15–17]. Bose mixtures and dipolar Bose gases share similarities (competition between repulsive and attractive interactions), although the latter case is complicated by the anisotropy of the dipolar interaction.

A sufficiently large saturated droplet has a surface region where the density drops to zero and a uniform interior with a density plateau at the equilibrium density $\rho_{\rm eq}$ resulting from the balance of attractive and repulsive interactions. In this work we focus on the effect of self-binding rather than on the droplet surface. Therefore we take the thermodynamic limit $N \to \infty$ and $V \to \infty$ with $\rho = N/V$ fixed. We investigate the ground state of a three-dimensional uniform Bose mixture with partial densities ρ_1 and ρ_2 (hence a total density $\rho = \rho_1 + \rho_2$) and equal atom masses m. We explore a wide range of ρ_1 and ρ_2 values, finding an optimal ratio ρ_1/ρ_2 and the equilibrium density $\rho_{\rm eq}$. We note, however, that in the presently published experiments [6,7], the self-bound droplets are not saturated: they do not exhibit a central density plateau but an approximately Gaussian density profile, and they are so small that they are dominated by surface effects.

The Hamiltonian of a Bose mixture is given by

$$H = -\sum_{i,\alpha} \frac{\hbar^2}{2m}\Delta_{i,\alpha} + \frac{1}{2}\sum_{\alpha,\beta}{\sum_{i,j}}' v_{\alpha,\beta}(|\mathbf{r}_{i,\alpha} - \mathbf{r}_{j,\beta}|), \quad (1)$$

where a Greek index α labels the component, and a Latin index i numbers the atoms of species α. The prime indicates that we only sum over $i \neq j$ for $\alpha = \beta$. We use the Lennard–Jones-like interactions

$$v_{\alpha,\beta}(r) = s_{\alpha,\beta}\left[\left(\frac{\sigma_{\alpha,\beta}}{r}\right)^{10} - \left(\frac{\sigma_{\alpha,\beta}}{r}\right)^{6}\right],$$

with $v_{12} = v_{21}$. The parameters of $v_{\alpha,\beta}$ are adjusted to set the s-wave scattering length $a_{\alpha,\beta}$ to a desired value, which can be done analytically [18]. Since $v_{\alpha,\beta}$ has two parameters, we further characterize $v_{\alpha,\beta}(r)$ by the effective range $r^{\rm eff}_{\alpha,\beta}$, evaluated numerically [19]. In all calculations, $s_{\alpha,\beta}$ and $\sigma_{\alpha,\beta}$ are chosen such that there are no two-body bound states.

Previously, Lee–Huang–Yang corrections to the mean-field approximation [5] and quantum Monte Carlo (QMC) methods [20,21] have been employed. Here we use a different approach, the variational hypernetted-chain Euler–Lagrange (HNC-EL) method. HNC-EL is computationally very economical, like the BMF approximation, but has the advantage of including correlations in a nonperturbative manner. This leads to a strictly real ground-state energy, in contrast to the BMF approximation where the energy of a uniform self-bound mixture has an unphysical small imaginary part. The two-component HNC-EL method has been described in Ref. [22]

and in a different formulation in Ref. [23], and has been recently generalized to multicomponent Bose mixtures [24]. The starting point is the variational Jastrow–Feenberg ansatz [25] for the ground state consisting of a product of pair correlation functions for a multicomponent Bose system,

$$\Psi_0(\{\mathbf{r}_{i,\alpha}\}) = \exp\left[\frac{1}{4}\sum_{\alpha,\beta}\sum_{i,j}{}' u_{\alpha,\beta}(|\mathbf{r}_{i,\alpha}-\mathbf{r}_{j,\beta}|)\right]. \quad (2)$$

The many-body wave function Ψ_0 does not contain one-body functions $u_\alpha(\mathbf{r}_{i,\alpha})$ because we consider a uniform system. Higher-order correlations such as triplets $u_{\alpha,\beta,\gamma}(\mathbf{r}_{i,\alpha},\mathbf{r}_{j,\beta},\mathbf{r}_{k,\gamma})$ have been incorporated approximately for helium [26,27], but are neglected here because their contribution is very small at low density.

We solve the Euler–Lagrange equations $\delta e/\delta g_{\alpha,\beta}(r) = 0$, where the energy per particle $e = \frac{1}{N}\frac{\langle\Psi_0|H|\Psi_0\rangle}{\langle\Psi_0|\Psi_0\rangle}$ is

$$e = \sum_{\alpha,\beta}\frac{\rho_\alpha\rho_\beta}{2\rho}\int d^3r\, g_{\alpha,\beta}(r)\left[v_{\alpha,\beta}(r) - \frac{\hbar^2}{4m}\Delta u_{\alpha,\beta}(r)\right] \quad (3)$$

in terms of the pair distribution function

$$g_{\alpha,\beta}(r) = \frac{1+\delta_{\alpha\beta}}{\rho_\alpha\rho_\beta}\frac{\delta\ln\langle\Psi_0|\Psi_0\rangle}{\delta u_{\alpha,\beta}}.$$

Partial summation of the Meyer cluster diagrams for $\ln\langle\Psi_0|\Psi_0\rangle$ in the HNC/0 approximation provides a relation between $g_{\alpha,\beta}$ and $u_{\alpha,\beta}$ [28,29]. A practical formulation of the resulting HNC-EL equations to be solved for $g_{\alpha,\beta}$ can be found in Ref. [24]. From $g_{\alpha,\beta}(r)$ we can calculate the static structure functions $S_{\alpha,\beta}(k) = \delta_{\alpha\beta} + \sqrt{\rho_\alpha\rho_\beta}\ \mathrm{FT}[g_{\alpha,\beta}-1]$ (FT denotes Fourier transformation), needed for the calculation of excitations.

At low densities, a uniform binary Bose mixture of two species of equal mass is characterized by the scattering lengths a_{11}, a_{12}, and a_{22}, and the partial densities ρ_1 and ρ_2. However, our results depend also on the next term in the expansion of the scattering phase shift, the effective range $r^{\mathrm{eff}}_{\alpha,\beta}$ [30], leading to a total of eight parameters $\{\rho_\alpha, a_{\alpha,\beta}, r^{\mathrm{eff}}_{\alpha,\beta}\}$ to characterize our uniform binary Bose mixtures. We use a_{11} as the length unit and $E_0 \equiv \hbar^2/ma_{11}^2$ as the energy unit. For ^{39}K used in experiments [6,7], we have $a_{11} = 35.2a_B$ and $E_0 = 3.55$ mK. We have used these values to restore dimensions in some of the figures below.

We use the combinations of scattering lengths $a_{\alpha\beta}$ from the experiments reported in Ref. [6], which are very similar to those reported in Ref. [7]. A negative value of $\delta a = a_{12} + \sqrt{a_{11}a_{22}}$ is necessary for a self-bound mixture. Before investigating the dependence on δa, we study the dependence on the partial densities ρ_1 and ρ_2. Figure 1 shows a map of the energy per particle e as function of ρ_1 and ρ_2 for the experimental scattering lengths corresponding to $\delta a = -5.5a_B$, which is $\delta a = -0.156$ in our length unit a_{11} and the most negative value in Ref. [6]. The other scattering lengths are $a_{22} = 1.86$ and $a_{12} = -1.52$. The effective ranges are $r^{\mathrm{eff}}_{11} = 5.2$, $r^{\mathrm{eff}}_{12} = 33.0$, and $r^{\mathrm{eff}}_{22} = 43.2$. Negative energies, where the mixture is a self-bound liquid, are shown by a red color range, together with contour lines, positive energies by a blue color range. Thus, as predicted by BMF calculations [5] and confirmed by experiments [6,7], we find a liquid state for $\delta a < 0$. In the phase space (ρ_1, ρ_2) the self-bound states form a narrow valley following a typical optimal ratio ρ_1/ρ_2. The phase space of meaningful combinations (ρ_1, ρ_2) ends at the spinodal line (thick black line in Fig. 1). Approaching this line, the *uniform* mixture becomes sensitive to long-wavelength density oscillations (see below). At the spinodal line, infinitesimal density fluctuations trigger a liquid-gas phase separation.

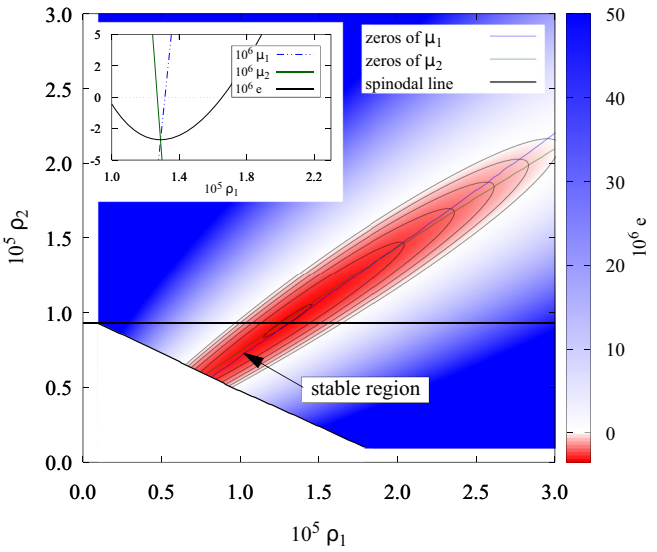

FIG. 1. Total energy per particle e as a function of ρ_1 and ρ_2 for $\delta a = -5.5a_B$, with contour lines for energies -3.35, -2.68, -2.01, -1.34, -0.67, and 0.0 Also shown are the spinodal instability (thick black line), and the zeros of the chemical potentials μ_1 (blue) and μ_2 (green). Only in the narrow region pointed at by the arrow is the mixture stable against evaporation. The inset shows e and the chemical potentials μ_1 and μ_2 along the dashed line intersecting the energy minimum.

While in a uniform mixture we can choose any ρ_1 and ρ_1, a finite droplet adjusts its radius to minimize the energy, attaining the equilibrium (zero pressure) density inside the droplet. The situation is more complicated for a mixture because the droplet radius affects only the total density, but not necessarily the ratio ρ_1/ρ_2. The latter can be adjusted by evaporating one component or by phase separation. Therefore, we calculate the chemical potential of component α, $\mu_\alpha(\rho_1,\rho_2) = e(\rho_1,\rho_2) + \rho\frac{\partial e(\rho_1,\rho_2)}{\partial\rho_\alpha}$. If $\mu_\alpha > 0$ a particle of species α is not bound to the mixture—the energy is lowered by removing it. A stable droplet requires both $e < 0$ (red valley in Fig. 1) and $\mu_\alpha < 0$. The blue line in Fig. 1 shows the zeros of μ_1, with $\mu_1 < 0$ *above* this line. Similarly the green line shows the zeros of μ_2, with $\mu_2 < 0$ *below* this line. Hence only the narrow region pointed at by the arrow is stable against evaporation; this region includes of course the equilibrium energy $e_{\mathrm{eq}} = \min[e]$. The inset of Fig. 1 shows e, μ_1, and μ_2 along the dashed line as function of ρ_1 for a fixed value $\rho_2 a_{11}^3 = 0.934\times10^{-5}$, such that we intersect the equilibrium energy. μ_α is very sensitive to the partial density, which explains why the region where both $\mu_\alpha < 0$ is so narrow. If a droplet is prepared outside the stable region, particles evaporate and the system moves on the energy surface until it is stable.

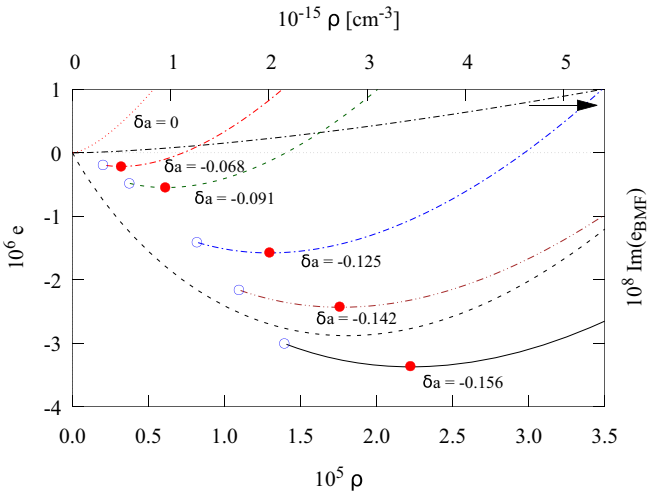

FIG. 2. Energy per particle e as function of the total density ρ for several values δa. Closed circles denote the equilibrium density $\rho_{\rm eq}$ and energy $e_{\rm eq}$; open circles denote spinodal points. The black dashed and dash-dotted lines are the real and imaginary parts, the latter using a different scale, of the BMF energy for $\delta a = -0.156$.

Our results for e and μ_α mean that large droplets will reach the equilibrium energy $e_{\rm eq}$ by a combination of evaporating superfluous particles and adjusting the droplet radius. In the case discussed so far, $\delta a = -0.156$, the density ratio at the equilibrium energy predicted from our HNC-EL results in Fig. 1 is $\rho_1/\rho_2 = 1.380$, which is to be compared with the optimal mean-field ratio [31] $\rho_1/\rho_2 = \sqrt{a_{22}/a_{11}} = 1.363$. The latter is a very good approximation even though the mean-field approximation does not even predict a liquid state. As seen in the inset of Fig. 1, e changes very little if the density ratio is slightly changed; therefore for further calculations of e we use the mean-field ratio.

When δa increases towards zero, the liquid becomes less bound, until it is no longer self-bound at $\delta a = 0$. In Fig. 2 the energy per particle e as function of total density ρ is shown for several values of δa in the range $[-0.156, 0]$, corresponding to the range of values in experiments [6,7] where δa is adjusted by changing the s-wave scattering length a_{22} via a magnetic field. We follow this protocol and modify the strength s_{22} of $v_{22}(r)$ to obtain the corresponding a_{22}, which also changes $r_{22}^{\rm eff}$; v_{11} and v_{12} are not changed and chosen as above. Table I lists the values of a_{22}, $r_{22}^{\rm eff}$, and ρ_1/ρ_2 for Fig. 2. The equilibrium energies $e_{\rm eq}$ and densities $\rho_{\rm eq}$ are marked by filled circles and are also listed in Table I. Naturally, both $e_{\rm eq} \to 0$ and $\rho_{\rm eq} \to 0$ as $\delta a \to 0$. For $\delta a = 0$, $e > 0$ and the mixture is not liquid anymore. The spinodal densities, where a uniform liquid becomes unstable against infinitesimal density fluctuations, are marked by open circles in Fig. 2. Also shown in Fig. 2 is the energy per particle $e_{\rm BMF}$ calculated in the BMF approximation [5] for $\delta a = -0.156$. Since $e_{\rm BMF}$ is complex, we show both the real and the small imaginary part of $e_{\rm BMF}$ (note the different energy scale for the latter). The BMF approximation fails to predict the spinodal instability and $e_{\rm BMF}$ extends all the way to $\rho = 0$.

TABLE I. Values for δa, a_{22}, $r_{22}^{\rm eff}$, and ρ_1/ρ_2 used to obtain the results shown in Fig. 2, as well as the equilibrium energy and density obtained from these results. Lengths and energies are in units of a_{11} and E_0 (see text) if not otherwise stated.

δa [units of a_B]	δa	a_{22}	$r_{22}^{\rm eff}$	ρ_1/ρ_2	$10^6 e_{\rm eq}$	$10^5 \rho_{\rm eq}$
−5.5	−0.156	1.86	43.2	1.363	−3.364	2.221
−5.0	−0.142	1.90	40.3	1.377	−2.426	1.756
−4.4	−0.125	1.94	37.0	1.394	−1.571	1.294
−3.2	−0.091	2.04	31.2	1.428	−0.544	0.609
−2.4	−0.068	2.10	27.7	1.450	−0.214	0.319
0.0	0.0	2.31	19.1	1.519		

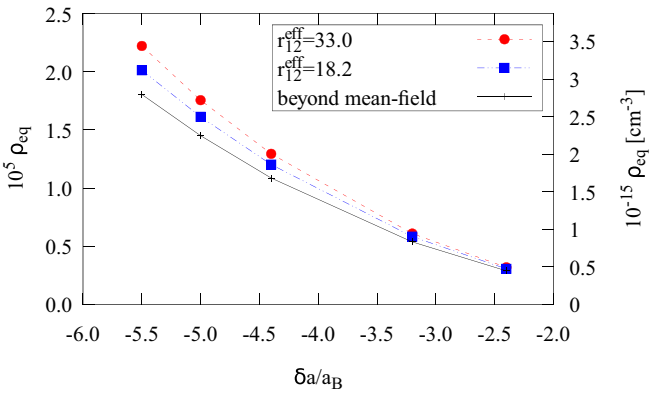

FIG. 3. Equilibrium density $\rho_{\rm eq}$ of the uniform Bose mixture as function of δa, varied by changing a_{22}; see Table I. For all curves, $a_{12} = -1.52$. The circles and squares are the present HNC-EL results obtained for $r_{12}^{\rm eff} = 33.0$ and 18.2, respectively. The line is the BMF result.

The density is more accessible to measurement than the energy; e.g., in Refs. [6,7] the central density of droplets was measured. In Fig. 3 we summarize the results shown in Fig. 2 by plotting the equilibrium total density $\rho_{\rm eq}$ as a function of δa (filled circles). Also shown in Fig. 3 is the BMF result for $\rho_{\rm eq}(\delta a)$, obtained as the minimum of the real part of the BMF energy, which qualitatively agrees with HNC-EL but predicts a somewhat lower equilibrium density. The square symbols in Fig. 3 show our results for $\rho_{\rm eq}(\delta a)$, if we choose different parameters s_{12} and σ_{12} in $v_{12}(r)$ such that we keep $a_{12} = -1.519$, while changing the effective range from $r_{12}^{\rm eff} = 33.0$ (upper curve) to $r_{12}^{\rm eff} = 18.2$ (lower curve). This demonstrates that the results are not universal; they depend not only the s-wave scattering lengths, but at least also on the effective ranges.

Figure 4 shows the dependence of the energy per particle $e(\rho)$ on the effective range $r_{12}^{\rm eff}$ for $\delta a = -0.156$, with $a_{12} = -1.519$ and the other scattering lengths as above, for different values $r_{12}^{\rm eff} = 18.2$, 23.0, 33.0, 44.8. The dependence on $r_{12}^{\rm eff}$ is significant, with e varying by 10% and $\rho_{\rm eq}$ varying by 13% for this range of $r_{12}^{\rm eff}$ values. The BMF energy Re$[e_{\rm BMF}]$ agrees better with HNC-EL for smaller $r_{12}^{\rm eff}$. Alkali interaction potentials have an effective range that is often much larger than the s-wave scattering length [32]. The values of $r_{12}^{\rm eff}$ [33] used here are of the order of those relevant to the ^{39}K experiments of Refs. [6,7,10], computed according to the model of Ref. [34]. Considering the low equilibrium densities $\rho_{\rm eq}$, it might appear surprising to find this nonuniversal behavior. We note, however, that for small δa the mean-field energy is the result of large

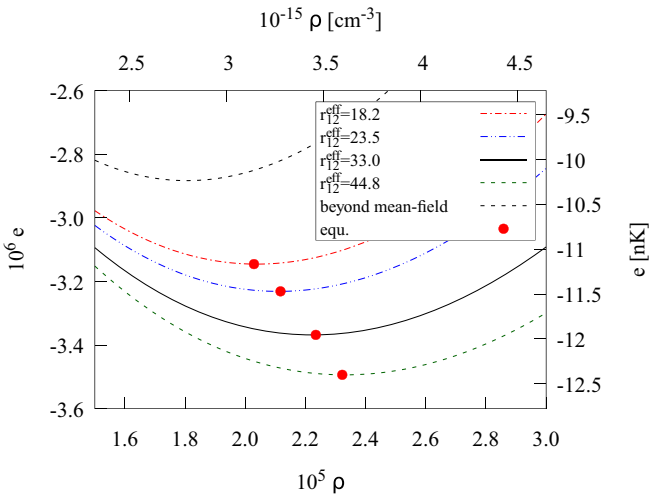

FIG. 4. $e(\rho)$ for $\delta a = -0.156$ and four models for the interspecies interaction v_{12} corresponding to effective ranges $r_{12}^{\rm eff} = 18.2$, 23.0, 33.0, 44.8. Also shown is the BMF result Re$[e_{\rm BMF}]$.

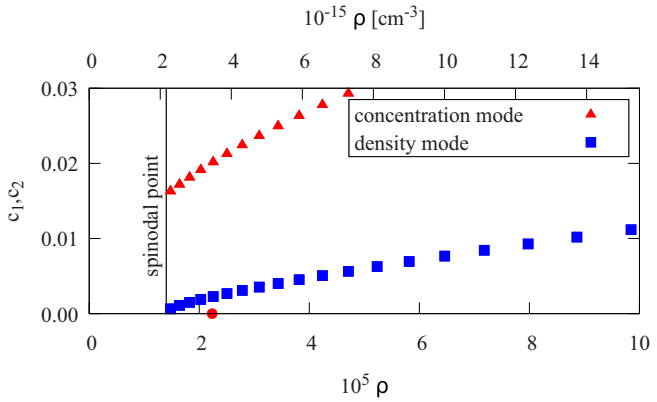

FIG. 5. Long-wavelength phase velocities in the two-component Bijl–Feynman approximation for density oscillations (lower curve) and concentration oscillations (upper curve) as a function of total density. The vertical line denotes the spinodal instability, and the red circle denotes the equilibrium density.

cancellations of negative and positive contributions. Therefore, it is plausible that a dependence on higher-order parameters such as the effective range becomes visible.

The spinodal instability (thick black line in Fig. 1) can be relevant for the preparation of the liquid droplets, achieved by ramping one of the scattering lengths. During a fast ramp, the mixture may visit the "forbidden" region of the (ρ_1, ρ_2) phase space and can condense into multiple droplets. To characterize the uniform liquid mixture near this instability in more detail, we choose $a_{\alpha,\beta}$ and $r_{\alpha,\beta}^{\rm eff}$ as for Fig. 1 corresponding to $\delta a = -0.156$, and the mean-field optimal ratio $\rho_1/\rho_2 = 1.363$. A simple approximation for the excitation spectrum of a Bose mixture is given by the Bijl–Feynman approximation [35], which provides a good estimate of the long-wavelength dispersion. A mixture supports density and concentration oscillations, with dispersion relations $\epsilon_1(k)$ and $\epsilon_2(k)$, respectively. They can be easily calculated from the static structure functions $S_{\alpha\beta}(k)$ by solving the eigenvalue problem $\frac{\hbar^2 k^2}{2m}\boldsymbol{\psi}_i = \epsilon_i(k)\mathbf{S}(k)\boldsymbol{\psi}_i$ where $\mathbf{S}$ is the 2×2 matrix with elements $S_{\alpha\beta}(k)$ and $\boldsymbol{\psi}_i$ are two-component vectors. Figure 5 shows the long-wavelength phase velocities $c_i = \lim_{k\to 0} d\epsilon_i(k)/dk$ for the density and concentration mode. The density mode has lower energy than the concentration mode for all densities shown in Fig. 5, including the equilibrium density. While c_2 is finite and hence the mixture is stable against demixing, the density mode becomes soft for $k \to 0$ as ρ is lowered, evidenced by the vanishing speed of sound c_1 at the spinodal instability (vertical line), where phase separation into liquid and gas occurs. This is similar to the onset of the modulational instability in dipolar Bose gases [11,12], which however is triggered by a vanishing roton energy with a *finite* wave number [36,37]. Excitations of Bose mixtures were also studied using Beliaev diagrammatic theory [38].

In summary, we analyze the properties of a liquid, i.e., self-bound, uniform Bose mixture using s-wave scattering lengths as in Refs. [6,7]. With the HNC-EL method, which includes pair correlations nonperturbatively, we find a narrow regime of partial densities ρ_α where the conditions for a stable liquid mixture are met: the energy per particle and both chemical potentials $\mu_\alpha(\rho_1, \rho_2)$ are negative. If $\mu_\alpha > 0$, atoms of component α evaporate until reaching either equilibrium or the spinodal line. Despite their ultralow density, the properties of these liquids depend also on the effective ranges $r_{\alpha,\beta}^{\rm eff}$. This deviation from universality was not observed in two-dimensional liquids [20]. We find that the liquid can have a spinodal instability, where the speed of sound vanishes and infinitesimal density fluctuations lead to a separation into a liquid and gas phase, which can be relevant during a nonadiabatic evolution of a droplet in experiments. We compare our HNC-EL results with the BMF approximation and find qualitative agreement, the small differences in energies and equilibrium densities can probably be attributed to the neglect of the effective range in the BMF approximation. However, as a low-density expansion, BMF misses the spinodal point and leads to a small but unphysical imaginary part in the energy for $\delta a < 0$, while the HNC-EL energies are always real. The existence of the spinodal point demonstrates quite well why the BMF approximation, which relies on the LHY low-density expansion in a local density approximation, is conceptually unpleasant: a uniform liquid phase does not exist for low densities because of the spinodal point; see Fig. 1. In the presently available experiments [6,7] the liquid droplets are far from saturation, as evidenced by the Gaussian shaped density profiles, and possibly not in equilibrium. Describing small unsaturated droplets will require an inhomogeneous generalization of HNC-EL based on the energy functional (3).

We acknowledge discussions with Leticia Tarruell, Leandra Vranješ Markić, Gregory Astrakharchik, Manuel Barranco, and Francesco Ancilotto, and financial support by the Austrian Science Fund FWF (Grant No. P23535-N20).

[1] I. Bloch, J. Dalibard, and W. Zwerger, Rev. Mod. Phys. **80**, 885 (2008).

[2] A. Micheli, G. K. Brennen, and P. Zoller, Nat. Phys. **2**, 341 (2006).

[3] I. Bloch, Nat. Phys. **1**, 23 (2005).

[4] M. Randeria, W. Zwerger, and M. Zwierlein, in *The BCS-BEC Crossover and the Unitary Fermi Gas*, edited by W. Zwerger Lecture Notes in Physics (Springer, Berlin, 2012), Vol. 836, pp. 1–32.

[5] D. S. Petrov, Phys. Rev. Lett. **115**, 155302 (2015).

[6] C. R. Cabrera, L. Tanzi, J. Sanz, B. Naylor, P. Thomas, P. Cheiney, and L. Tarruell, Science **359**, 301 (2018).

[7] G. Semeghini, G. Ferioli, L. Masi, C. Mazzinghi, L. Wolswijk, F. Minardi, M. Modugno, G. Modugno, M. Inguscio, and M. Fattori, Phys. Rev. Lett. **120**, 235301 (2018).

[8] F. Dalfovo, S. Giorgini, L. P. Pitaevskii, and S. Stringari, Rev. Mod. Phys. **71**, 463 (1999).

[9] D. M. Larsen, Ann. Phys. (NY) **24**, 89 (1963).

[10] P. Cheiney, C. R. Cabrera, J. Sanz, B. Naylor, L. Tanzi, and L. Tarruell, Phys. Rev. Lett. **120**, 135301 (2018).

[11] H. Kadau, M. Schmitt, M. Wenzel, C. Wink, T. Maier, I. Ferrier-Barbut, and T. Pfau, Nature (London) **530**, 194 (2016).

[12] I. Ferrier-Barbut, H. Kadau, M. Schmitt, M. Wenzel, and T. Pfau, Phys. Rev. Lett. **116**, 215301 (2016).

[13] M. Schmitt, M. Wenzel, F. Böttcher, I. Ferrier-Barbut, and T. Pfau, Nature (London) **539**, 259 (2016).

[14] L. Chomaz, S. Baier, D. Petter, M. J. Mark, F. Wächtler, L. Santos, and F. Ferlaino, Phys. Rev. X **6**, 041039 (2016).

[15] F. Wächtler and L. Santos, Phys. Rev. A **93**, 061603 (2016).

[16] D. Baillie, R. M. Wilson, R. N. Bisset, and P. B. Blakie, Phys. Rev. A **94**, 021602 (2016).

[17] R. Bombin, J. Boronat, and F. Mazzanti, Phys. Rev. Lett. **119**, 250402 (2017).

[18] J. Pade, Eur. Phys. J. D **44**, 345 (2007).

[19] E. Buendia, R. Guardiola, and M. de Llano, Phys. Rev. A **30**, 941 (1984).

[20] D. S. Petrov and G. E. Astrakharchik, Phys. Rev. Lett. **117**, 100401 (2016).

[21] V. Cikojevic, K. Dzelalija, P. Stipanovic, L. Vranjes Markic, and J. Boronat, Phys. Rev. B **97**, 140502 (2018).

[22] T. Chakraborty, Phys. Rev. B **26**, 6131 (1982).

[23] C. Campbell, Ann. Phys. (NY) **74**, 43 (1972).

[24] M. Hebenstreit, M. Rader, and R. E. Zillich, Phys. Rev. A **93**, 013611 (2016).

[25] E. Feenberg, *Theory of Quantum Fluids* (Academic Press, London, 1969).

[26] A. Fabrocini and A. Polls, Phys. Rev. B **30**, 1200 (1984).

[27] E. Krotscheck, Phys. Rev. B **33**, 3158 (1986).

[28] J. P. Hansen and I. R. McDonald, *Theory of Simple Liquids* (Academic Press, London, 1986).

[29] M. Hebenstreit, B.S. Thesis, Johannes Kepler University, 2013 (unpublished).

[30] L. D. Landau and E. M. Lifshitz, *Quantum Mechanics (Non-relativistic Theory)*, Course of Theoretical Physics (Pergamon Press, London, 1958), Vol. III.

[31] C. J. Pethick and H. Smith, *Bose-Einstein Condensation in Dilute Gases* (Cambridge University Press, Cambridge, 2008).

[32] V. V. Flambaum, G. F. Gribakin, and C. Harabati, Phys. Rev. A **59**, 1998 (1999).

[33] A. Simoni (private communication).

[34] S. Roy, M. Landini, A. Trenkwalder, G. Semeghini, G. Spagnolli, A. Simoni, M. Fattori, M. Inguscio, and G. Modugno, Phys. Rev. Lett. **111**, 053202 (2013).

[35] R. P. Feynman, Phys. Rev. **94**, 262 (1954).

[36] I. Ferrier-Barbut, M. Wenzel, M. Schmitt, F. Böttcher, and T. Pfau, Phys. Rev. A **97**, 011604 (2018).

[37] L. Chomaz, R. M. W. van Bijnen, D. Petter, G. Faraoni, S. Baier, J. H. Becher, M. J. Mark, F. Wächtler, L. Santos, and F. Ferlaino, Nat. Phys. **14**, 442 (2018).

[38] O. I. Utesov, M. I. Baglay, and S. V. Andreev, Phys. Rev. A **97**, 053617 (2018).